INSTITUTE OF PHYSICS PUBLISHING JOURNAL OF PHYSICS D: APPLIED PHYSICS
J. Phys. D: Appl. Phys. **35** (2002) 2676–2686 PII: S0022-3727(02)40065-4

Ricochet of a tungsten heavy alloy long-rod projectile from deformable steel plates

Woong Lee[1], **Heon-Joo Lee and Hyunho Shin**

Armoured Structure Division, Ground Systems Development Centre, Agency for Defence Development, PO Box 35-1, Yoosung, Taejeon 305-600, Republic of Korea

E-mail: wl10001@add.re.kr

Received 30 July 2002
Published 8 October 2002
Online at stacks.iop.org/JPhysD/35/2676

Abstract

Ricochet of a tungsten heavy alloy long-rod projectile from oblique steel plates with a finite thickness was investigated numerically using a full three-dimensional explicit finite element method. Three distinctive regimes resulting from oblique impact depending on the obliquity, namely simple ricochet, critical ricochet and target perforation, were investigated in detail. Critical ricochet angles were calculated for various impact velocities and strengths of the target plates. It was predicted that critical ricochet angle increases with decreasing impact velocities and that higher ricochet angles were expected if higher strength target materials are employed. Numerical predictions were compared with existing two-dimensional analytical models. Experiments were also carried out and the results supported the predictions of the numerical analysis.

1. Introduction

It is well known that a projectile impacting on a suitably inclined surface can bounce back from the surface or partially penetrate it (without perforating it and being stopped by it) along a curved trajectory on the impacted surface with a reduced velocity [1]. This phenomenon, known as ricochet, is controlled by such factors as properties of the materials constituting the projectiles and the impacted surfaces, impact velocity of the projectiles, and relative obliquity of the surfaces with respect to the impact path of the projectiles, etc [1]. Exploitation of ricochet to implement mass efficient means of armour protection is common in many military applications [2]. Despite numerous researches on ricochet of various types of projectiles from various types of surfaces [3–13], critical conditions for the ricochet of long-rod type projectiles has not been completely established yet.

On the extension of the series of investigations on the impact of long-rods on targets [14–16], Tate first described ricochet using a simplified two-dimensional hydrodynamic model [6]. For the geometry shown in figure 1, it was predicted that ricochet of a projectile with a square cross section would occur if

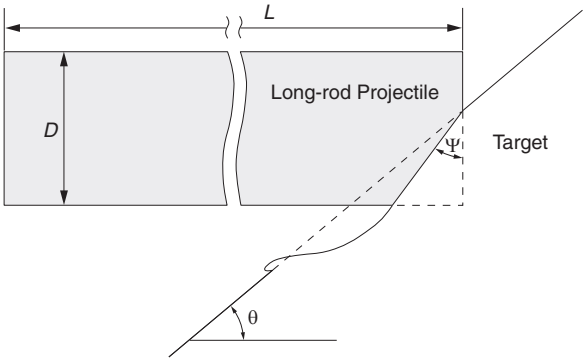

Figure 1. Basic geometry used for simple two-dimensional analysis for ricochet of long-rod type projectiles by Tate [6] and Rosenberg *et al* [7].

$$\tan^3\left(\frac{\pi}{2}-\theta\right) > \frac{2}{3}\frac{\rho_p v^2}{Y_p}\left(\frac{L}{D}+\frac{D}{L}\right)\left(1+\sqrt{\frac{\rho_p}{\rho_t}}\right) \quad (1)$$

where θ is the oblique angle, ρ_p and ρ_t are densities of the projectile and the target, respectively, v is the impact velocity, Y_p is the dynamic strength of the projectile and L and D

[1] Author to whom correspondence should be addressed.

are the length and diameter of the projectile, respectively. It is predicted from this expression that the higher projectile density, impact velocity and L/D ratio and lower rod strength will result in a lower ricochet angle.

However, in the derivation of equation (1), it was assumed that the projectile is a rigid body and that ricochet occurs due to the rotation of the projectile around its mass centre caused by the asymmetric reaction force exerted on its front from the impacted surface. These assumptions do not properly reflect physical phenomena predicted and observed in real systems, where the projectile bends on impact and then a plastic hinge forms, which travels backward with the progress of the projectile [1]. Further, equation (1) does not contain parameters representing geometry and mechanical properties of the target plate, which are believed to have some effects on the ricochet behaviour.

Rosenberg *et al* [7] supplemented some of these shortcomings by further including the effect of target strength and bending of the projectile. The ricochet condition suggested by them is (see figure 1 for the geometry)

$$\tan^2\left(\frac{\pi}{2}-\theta\right) > \frac{\rho_p v^2}{R_t}\left(\frac{v+u}{v-u}\right) \tag{2}$$

where R_t is the dynamic yield strength of the target and u is the penetration velocity which is expressed as [6]

$$u = \frac{\rho_p v - \sqrt{\rho_p^2 v^2 - (\rho_p - \rho_t)\left\{\rho_p v^2 + 2(Y_p - R_t)\right\}}}{\rho_p - \rho_t} \tag{3}$$

Though the theoretical model developed by Rosenberg *et al* includes the strength and density of both the target plate and the projectile, the L/D ratio of the projectile and thickness of the target plate are excluded. Comparison with experimental results showed that equation (2) formed a certain boundary between ricochet and penetration in terms of the ricochet angle expressed as a function of impact velocity, implying that the two-dimensional model could provide qualitative information regarding the ricochet condition. However, recent numerical analysis by Zukas and Gaskill [9], in which difference in two-dimensional and three-dimensional calculations on the ricochet of a square projectile with $L/D = 2$ were compared, suggested that two-dimensional plane strain analysis overestimates the critical ricochet angles and therefore should not be used for design purposes.

Further development of the analytical model for a full three-dimensional geometry seems to be a formidable task due to the complexity of the physics involved in the ricochet, which includes large-scale high-strain-rate elastoplastic deformation of the projectile and the target plate together with the erosion of both occurring in a very short period of time [1]. Thus, alternative approaches, use of experimental and numerical methods, have been used for more precise description of physical phenomena regarding ricochet by many researchers. Through a series of experiments on ricochet of long-rod projectiles made of modelling clay from a thick (undeformable) target, Johnson *et al* [10, 11] observed the formation of an asymmetric elliptical crater on the target surface due to oblique impact of the projectile. Elongation and subsequent fragmentation of the projectile were also observed to occur after ricochet. Reid *et al* [12] carried out experiments on the deformation behaviour of mild steel and aluminium long-rod projectiles striking at an undeformable oblique target and observed that the deformation of the projectiles consisted of impact end mushrooming and projectile buckling followed by its bending which terminated in a plastic hinge beyond which the projectile was not deformed.

In a numerical work on the ricochet of an annealed steel long-rod impacting on an oblique rolled homogenized armour (RHA) plate, Senf *et al* [8] predicted that the projectile bends on impacting the target plate and forms a plastic hinge which moves backward while its tip slides along the target surface. This prediction was supported by experimental observations. Bending of the projectile was also predicted from a numerical work of Jonas and Zukas [13], in which it was also reported that a two-dimensional model underestimated the projectile bending. However, these experimental and numerical works were mainly concerned with ricochet phenomenology from the viewpoint of the projectile behaviour rather than critical ricochet condition such as ricochet angles.

Some existing work on oblique impact [17–23] or near normal impact of the yawed projectiles [24–31] should also be noted. Although some useful information about the behaviour of the projectile and target during high-velocity impact can be obtained from these studies, they are focused more on the penetration and perforation process rather than the ricochet phenomena and, in particular, critical ricochet conditions. Especially, little attention has been paid to the problem of the ricochet of a tungsten heavy alloy (WHA) long-rod projectile, impacting at typical ordnance velocities, from a deformable RHA plate with finite thickness, the dimension of which is comparable to the diameter of the long-rod projectile, whilst this subject is of particular interest from the practical viewpoint. Thus, in the current study, ricochet phenomenology as well as the critical ricochet condition was numerically investigated for a real situation where a long-rod projectile impacts on oblique RHA and S-7 tool steel plates at various ordnance velocities. Experiments were also carried out to verify the numerical results.

2. Numerical analysis

A full three-dimensional explicit finite element analysis with Lagrangian formulation based on the principle of virtual work and the central difference time integration scheme [32, 33] was carried out to investigate the ricochet problem. Since theoretical and mathematical foundations for the explicit finite element analysis are well established [32, 33] and are widely adopted to solve the problem of high-strain-rate deformations [34], the lengthy derivation of the equations for the numerical analysis is not repeated here. A general-purpose explicit finite element analysis package MSC/DYTRAN[2] was used for the numerical calculations.

Figure 2 shows a typical finite element model used in the numerical analysis. The model consists of a rectangular oblique target plate and a cylindrically shaped projectile that is initially located 1 mm away from the target. Only half of the whole geometry was modelled due to the inherent symmetry of

[2] Product of the MacNeal-Schwendler Corp.

the model along the x-direction of the coordinate as shown in figure 2. The length and diameter of the projectiles chosen for the numerical analysis were 75 and 7 mm, respectively, giving an L/D ratio of 10.7. Impact velocities of the projectiles were varied from 1000 to 2000 m s^{-1} with an increment of 250 m s^{-1}. Target plates modelled are 150 mm long, 40 mm wide and 6.25 mm thick. Obliquity of the plates was varied from 3° to 25° with intervals of 1°. Typical eight-node linear brick elements with reduced integration were used for meshing as shown in figure 2. Material properties were applied to the model by assigning appropriate material properties to the pre-defined projectile and target element sets, i.e. properties of WHA to the projectile element set and properties of the two types of high hardness steel, namely, RHA class 4 [35] and S-7 tool steel [36], to the target element set.

In order to model a high-strain-rate mechanical response of the projectile and the target materials, a commonly used constitutive equation, the Johnson–Cook equation [36], was used as it is known to describe high-velocity mechanical response of a number of metals fairly well [37]. This has the form

$$\sigma = (\sigma_0 + B\varepsilon_{\mathrm{p}}^{n})\left(1 + C\ln\frac{\dot{\varepsilon}}{\dot{\varepsilon}_0}\right)\left[1 - \left(\frac{T - T_{\mathrm{r}}}{T_{\mathrm{m}} - T_{\mathrm{r}}}\right)^{m}\right] \quad (4)$$

where σ_0 is the static yield strength, ε_{p} the effective plastic strain, $\dot{\varepsilon}$ the effective strain rate, $\dot{\varepsilon}_0$ the reference strain rate, T the temperature, T_{r} the room temperature, T_{m} the melting temperature and B, C, m and n are material constants. For the materials used in this study, these parameters were determined from separate experiments (for RHA and WHA) or taken from Johnson and Cook (for S-7 tool steel) [36] and are shown in table 1 together with the basic physical properties required for the calculations.

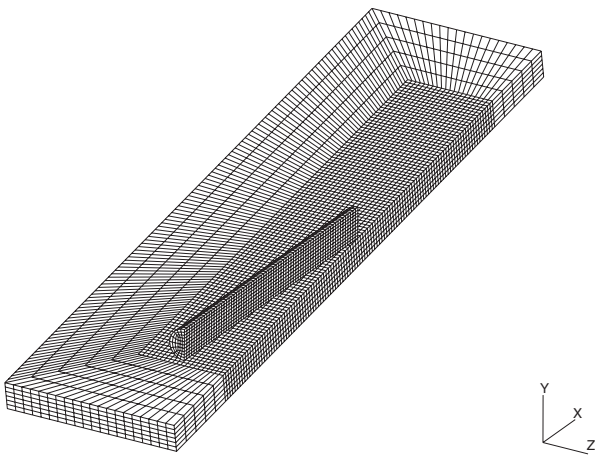

Figure 2. Typical finite element mesh coordinate system used for the numerical study in this work.

The interaction between the projectile and the plate was simulated by a Lagrangian–Lagrangian contact algorithm based on a slave-grid/master segment concept. This algorithm checks eventual penetration of slave-grids through master segments and applies constant forces to push them back. Erosion of the projectile and the target was simulated through a so-called adaptive contact algorithm [38], which automatically updates contact definition between the interacting deformable bodies upon elimination of the elements when pre-set level of plastic strains, determined by a separate depth of penetration (DOP) calibration, are reached.

3. Experimental

Experiments were carried out to verify the numerical results. The experimental set-up shown in figure 3 consists of three witness blocks (38 mm thick RHA class 4), an oblique target plate (6.25 mm thick RHA class 4), a velocity-measuring device and a solid propellant gun. WHA projectiles with L/D ratios of 10.7 ($L = 75$ and $D = 7$ mm) were impacted at velocities of about 1000 and 1500 m s^{-1}. The velocities of the projectiles were controlled by adjusting the amount of solid propellant charge. The relations between the amount of the charge and the projectile velocities were calibrated in a preparatory experiment.

4. Results and discussion

4.1. Post-impact behaviour of the projectile and the target plate

Numerical results are graphically shown in figures 4–6 in terms of the mesh deformation with the lapse of time to analyse the behaviour of the WHA projectile and the RHA target with thickness comparable to the projectile diameter during the oblique impact. When the projectile impact velocity is 1000 m s^{-1} and the target oblique angle is 10°, as in the case shown in figure 4, the projectile initially bends on impact (figure 4(*a*)). Subsequently, a plastic hinge is formed which remains at the initial point of impact with respect to a fixed coordinate system (Eulerian) resulting in its relative backward motion along the x-direction of the coordinate system (figure 2) as the projectile progresses forward (figures 4(*b*)–(*d*)). In the case being considered ($\theta = 10°$), where the oblique angle is lower than the critical ricochet angle, the target does not deform much and no significant erosion of the impacted surface is noticed whilst the front end (denoted as head hereinafter) of the projectile lifts from the target surface after sliding some distance and eventually the projectile bounces away (figures 4(*e*)–(*h*)). Such behaviour is yielded due to the asymmetric reaction force exerted from the contact area to the

Table 1. Material properties and constants for the Johnson–Cook model applied to the numerical model.

	Shear modulus (GPa)	ρ (kg m^{-3})	Specific heat (J kg^{-1} K^{-1})	$\dot{\varepsilon}_0$ (s^{-1})	T_{m} (K)	σ_0 (MPa)	B (MPa)	n	C	m
WHA	152.02	17 000	134	1	1723	1410	223.3	0.11	0.022	1.0
RHA	76.96	7 840	477	1	1809	1160	415.9	0.28	0.012	1.0
S-7	76.96	7 750	477	1	1763	1539	477	0.18	0.012	1.0

projectile, which is reportedly proportional to the area of the contact, target strength and oblique angle [6, 7, 12].

When the oblique angle of the target plate is increased to 12° whilst keeping the impact velocity the same, the projectile shows somewhat different behaviour. As shown in figures 5(*a*)–(*d*), it initially pushes the impacted area of the target inward following impact since the target plate is allowed to deform (bend). Whilst the head of the projectile tends to bounce back from the target due to the reaction force exerted from the contact area at the initial stage of the impact, its trailing portion (denoted as tail hereinafter) tends to penetrate into the target along an almost identical trajectory of the initial impact (figure 5(*e*)). Consequently, the front part ahead of the plastic hinge, which was bent and slid on the plate surface, bounces away whilst the rear part behind it penetrates into the deformed target forming a stretched section in the projectile and an impact crater in the target (figures 5(*f*) and (*g*)). Indeed, the relatively thin deformable target plays a significant role in yielding such phenomena. At the critical oblique angle, the tail also bounces away at a later time step before it completely perforates the target achieving critical ricochet (figure 5(*h*)). At this stage the elongation of the projectile becomes so severe that it results in the fragmentation of the projectile.

In the case where the oblique angle is further increased to 14° beyond the critical angle, as can be seen in figures 6(*a*)–(*d*), the initial behaviour of the projectile and the target is similar to the case of critical ricochet shown in figures 5(*a*)–(*d*).

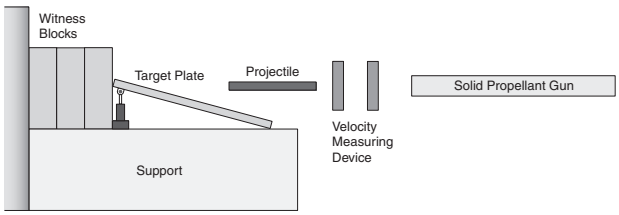

Figure 3. Schematic illustration of the experimental set-up for the observations of oblique impact of a long-rod projectile on a steel target plate performed in this study.

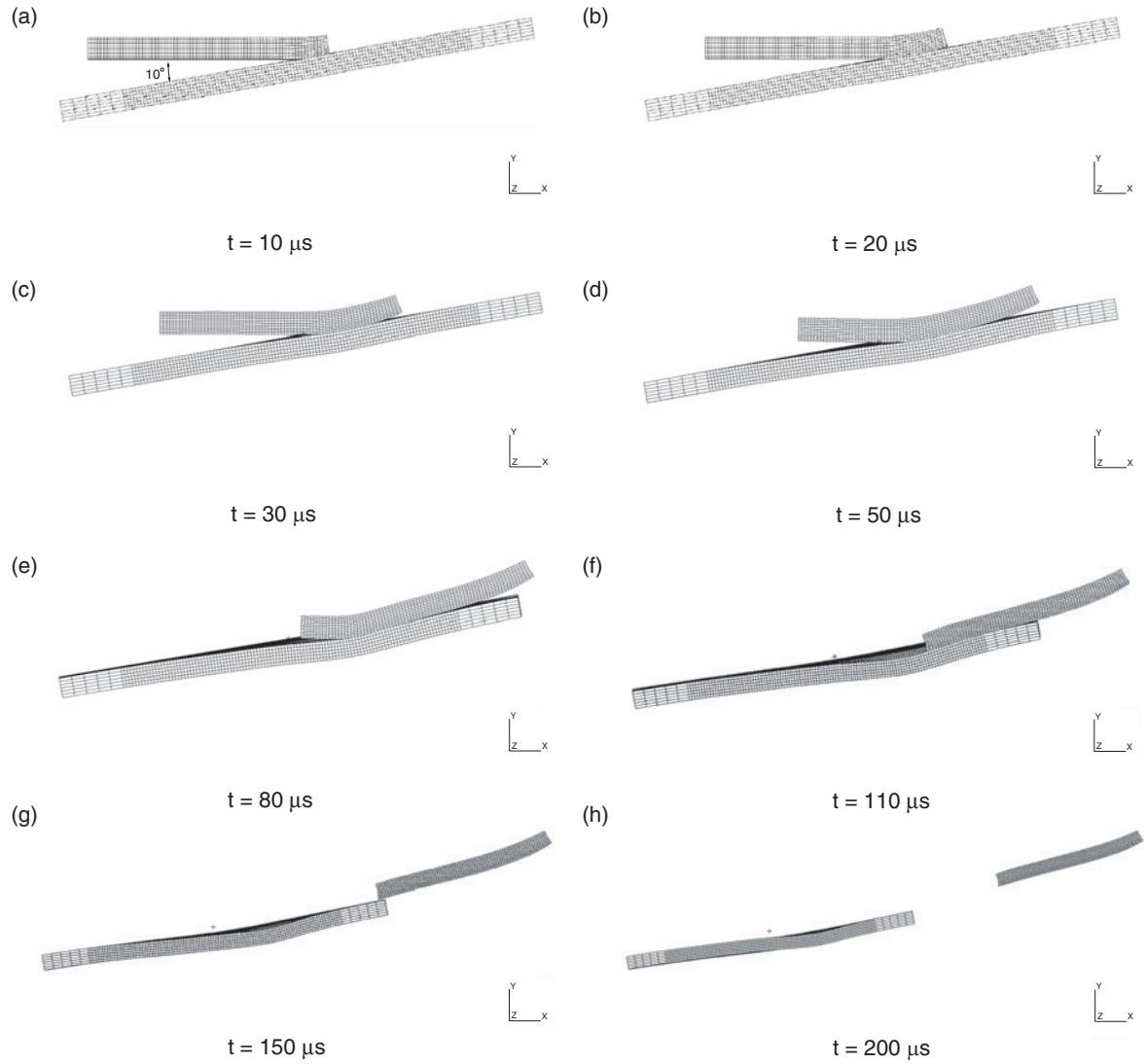

Figure 4. Numerical results showing the behaviour of the WHA projectile and the RHA target when the oblique angle is 10° and the impact velocity is 1000 m s^{-1}.

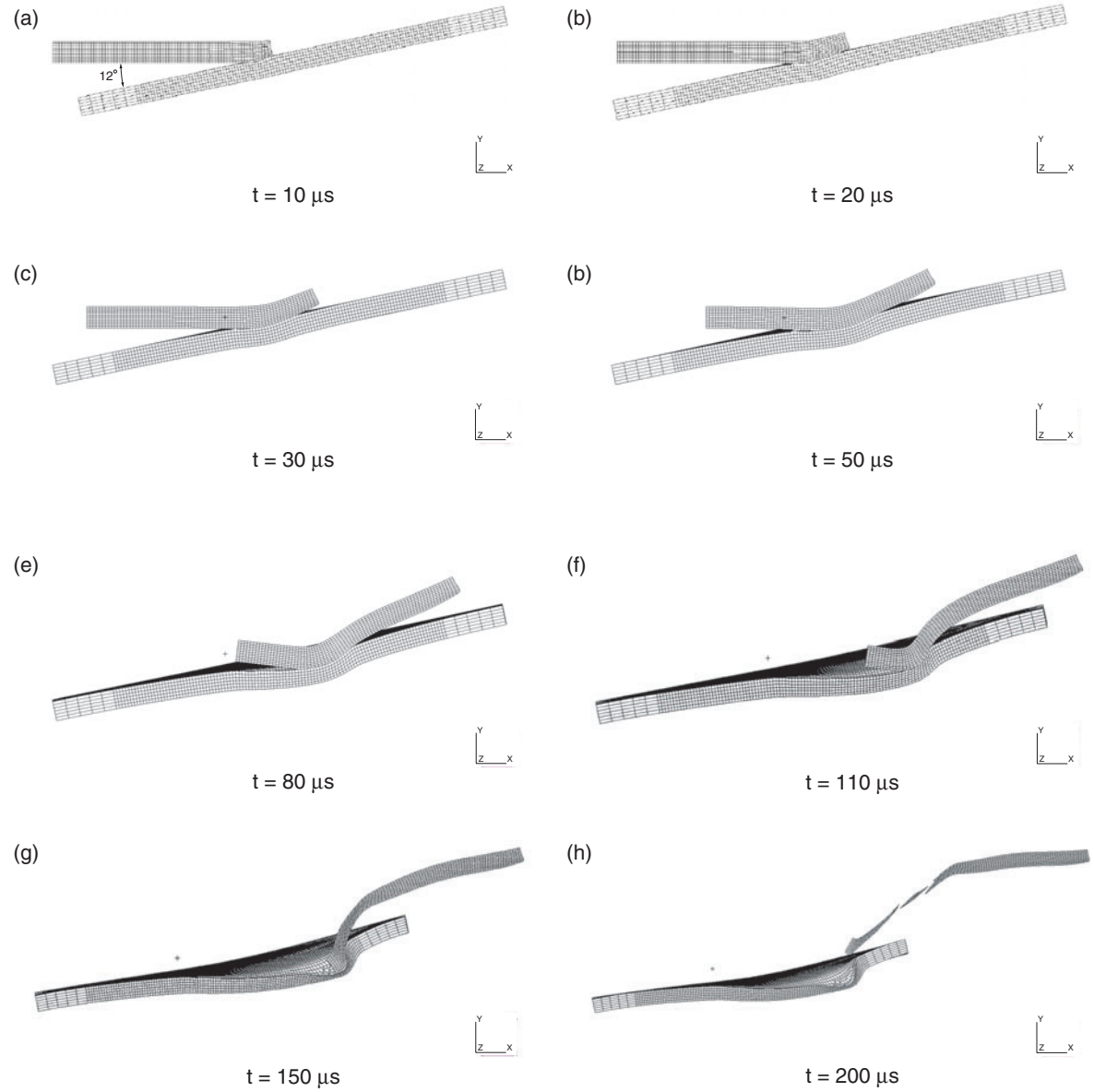

Figure 5. Numerical results showing the behaviour of the WHA projectile and the RHA target for the case of critical ricochet ($\theta = 12^{\circ}$ and $v = 1000\,\mathrm{m\,s^{-1}}$).

However, unlike in the previous case, the tail part further progresses to penetrate into the target downward by eroding it (figures 6(*e*) and (*f*)), resulting in the fragmentation of the projectile due to extreme elongation as well as complete penetration (perforation) of the target as shown in figures 6(*g*) and (*h*).

Understanding the physical nature of the above behaviour of the projectile and the target can be supplemented by analysing the changes in the projectile velocities after impact, as has also been performed for normal penetration in the literature [39–41]. For this purpose, post-impact changes in the horizontal (along the x-direction) and vertical (along the y-direction) velocities of head and tail of the projectile have been monitored during the numerical calculations and the results are plotted in figure 7. Before impact, the head and the tail move at the same initial velocity of $1000\,\mathrm{m\,s^{-1}}$ and there is no vertical velocity term. For the case with relatively low oblique angle, e.g. $\theta = 10^{\circ}$, as shown in figures 7(*a*) and (*b*), the horizontal velocities of the head and the tail of the projectile after impact are kept almost identical, implying no significant axial strain, which prevents the projectile segmentation. It can also be seen that the horizontal velocities did not decrease noticeably. From this, it is inferred that the projectile does not encounter any significant resistance to its motion along the flight trajectory and that the impact interaction of the projectile with the target does not cause any large-scale deformation of the target.

Whilst there were only slight changes in the horizontal velocities, vertical velocities of the head and the tail undergo noticeable changes during the impact process. As can be seen in figure 7(*a*), the vertical velocity of the head initially increases to about $260\,\mathrm{m\,s^{-1}}$ and remains almost the same thereafter, which would be associated with sliding on the target surface and subsequent takeoff of the head shown in figure 4. On the

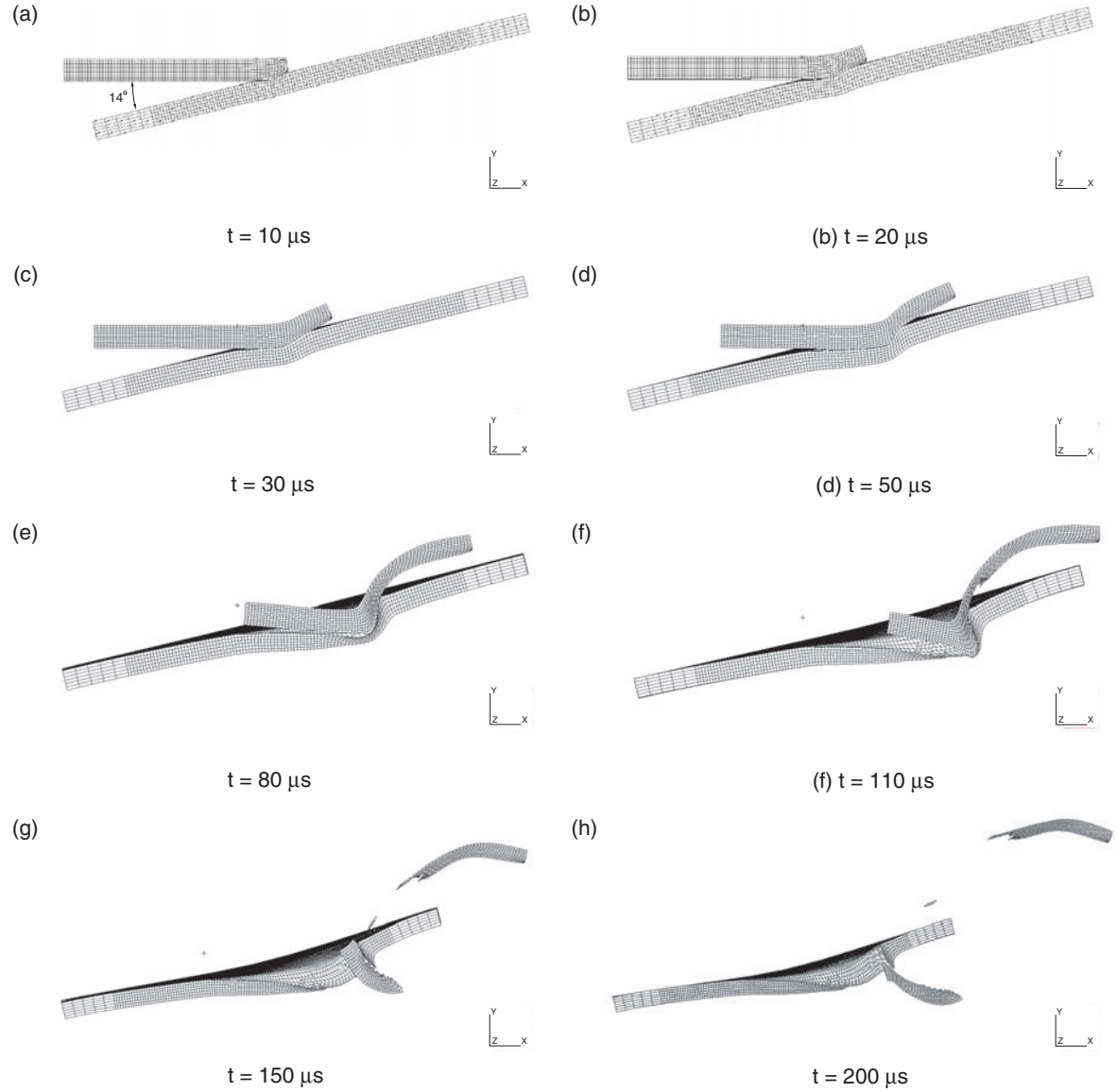

Figure 6. Numerical results showing the oblique impact process which leads to projectile segmentation and target perforation ($\theta = 14^{\circ}$ and $v = 1000\,\mathrm{m\,s^{-1}}$).

other hand, the vertical velocity of the tail is almost 0 until about 70 μs and then increases to about $320\,\mathrm{m\,s^{-1}}$ at 100 μs. This indicates that the impact of the head on the target does not cause any yawing force in the rear part of the projectile which is beyond the plastic hinge mentioned above. Near-constant vertical tail velocity of $250\,\mathrm{m\,s^{-1}}$ after about 120 μs would indicate the takeoff of the tail as shown in figures 4(*f*)–(*h*).

However, where critical ricochet was achieved ($\theta = 12^{\circ}$ for the case considered herein), as shown in figure 7(*c*), the decrease in the horizontal velocity of the head with respect to time is more pronounced than in the previous case, indicating that the progress of the head is hindered more. In particular, as shown in figure 7(*d*), the horizontal velocity of the tail decreases to almost 0 from about 140 μs, producing a velocity difference between the head and the tail of about $800\,\mathrm{m\,s^{-1}}$. Such a large velocity difference may cause large-scale deformation and therefore it would explain the stretching of the projectile shown in figure 5(*g*) followed by the segmentation of the projectile shown in figure 5(*h*). At the same time, a sudden drop in the horizontal velocity of the tail between 100 and 150 μs is believed to be related to the target cratering shown in figures 5(*f*) and (*g*), which could exert a high resistance to the advance of the tail. When critical ricochet is achieved, even though the impact crater is formed on the target, this does not lead to target perforation. This can be explained from the changes in the vertical velocities of the head and the tail shown in figures 7(*c*) and (*d*), where it can be seen that the head and the tail sequentially acquire positive, vertical velocity components. They begin to take off from the target plate at about 0 and 150 μs, respectively, indicating no further penetration of the target.

A similar trend is obtained when the target oblique angle is further increased, e.g. $\theta = 14^{\circ}$, as shown in figures 7(*e*) and (*f*) whilst two apparent differences are noticed. First, the horizontal velocity of the head, once it is decreased to about $700\,\mathrm{m\,s^{-1}}$ at about 120 μs, remains nearly constant implying

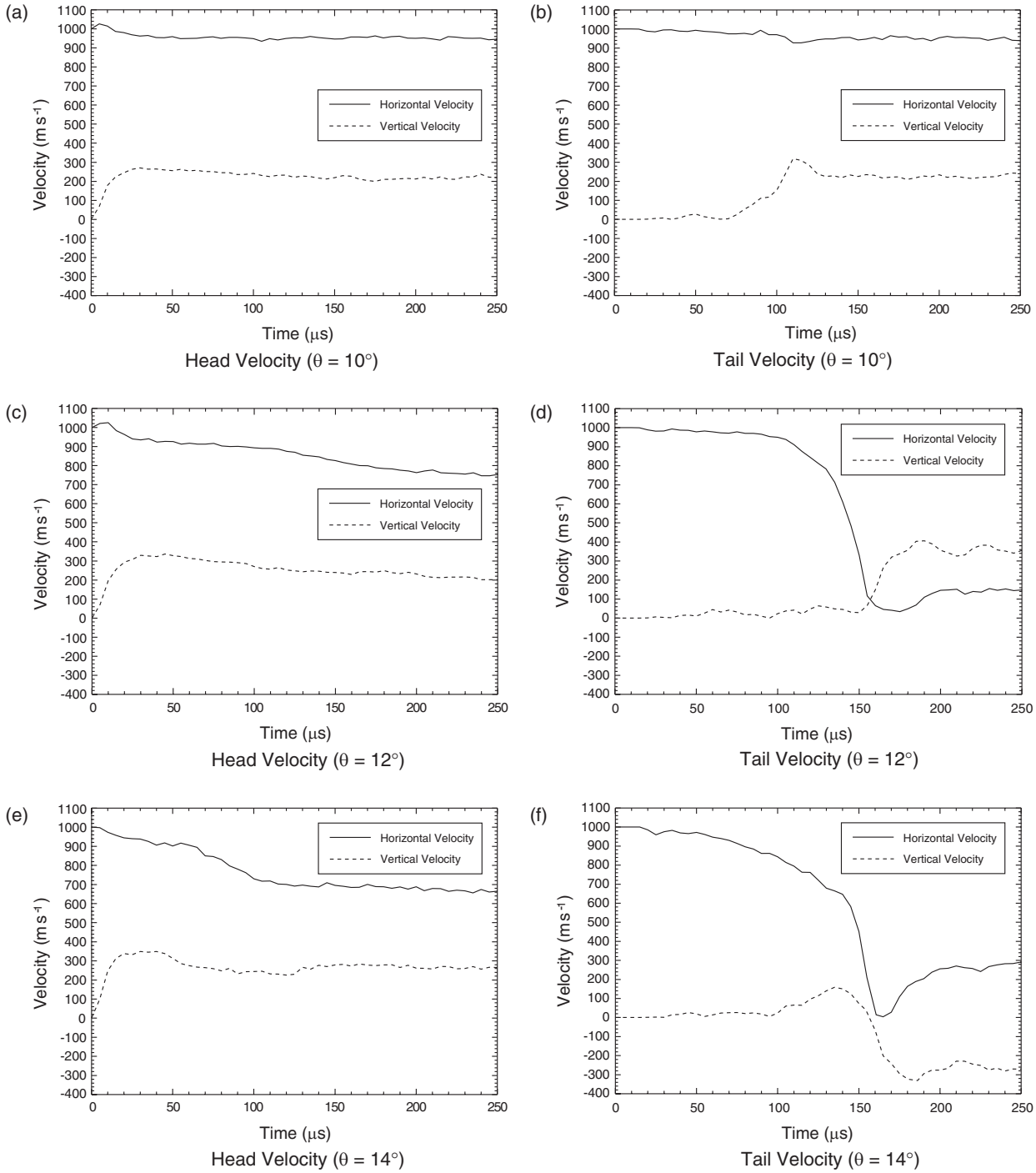

Figure 7. Post-impact changes in the horizontal and vertical velocities of the head and tail sections of the projectile impacting the target at $1000\,\mathrm{m\,s^{-1}}$.

that the flight of the head portion is no longer hindered by the target thereafter, probably due to the earlier segmentation of the projectile. In the previous case shown in figure 7(*c*), the head portion was connected to the tail portion through the elongated portion until the later time step so that the tail, still staying in the impact crater in the target, delayed the propagation of the head, which is represented as continuously decreasing velocity. Second, the behaviour of the tail after segmentation is completely different: the vertical velocity of the tail decreases to a negative value of about $-300\,\mathrm{m\,s^{-1}}$ from about $160\,\mu$s, which is then maintained almost constant after about $180\,\mu$s. This indicates that the fragmented tail is heading downward, which would be responsible for the perforation of the target shown in figure 6(*h*).

The ricochet behaviour illustrated in figures 4–6 are also supported by the experimentation carried out herein. Figure 8 shows the shape of the target plate and the witness block after the ricochet experiments. In this figure, the deformed shape of the plate is apparent with an asymmetric elliptical perforation hole. Occurrence of ricochet can be judged by

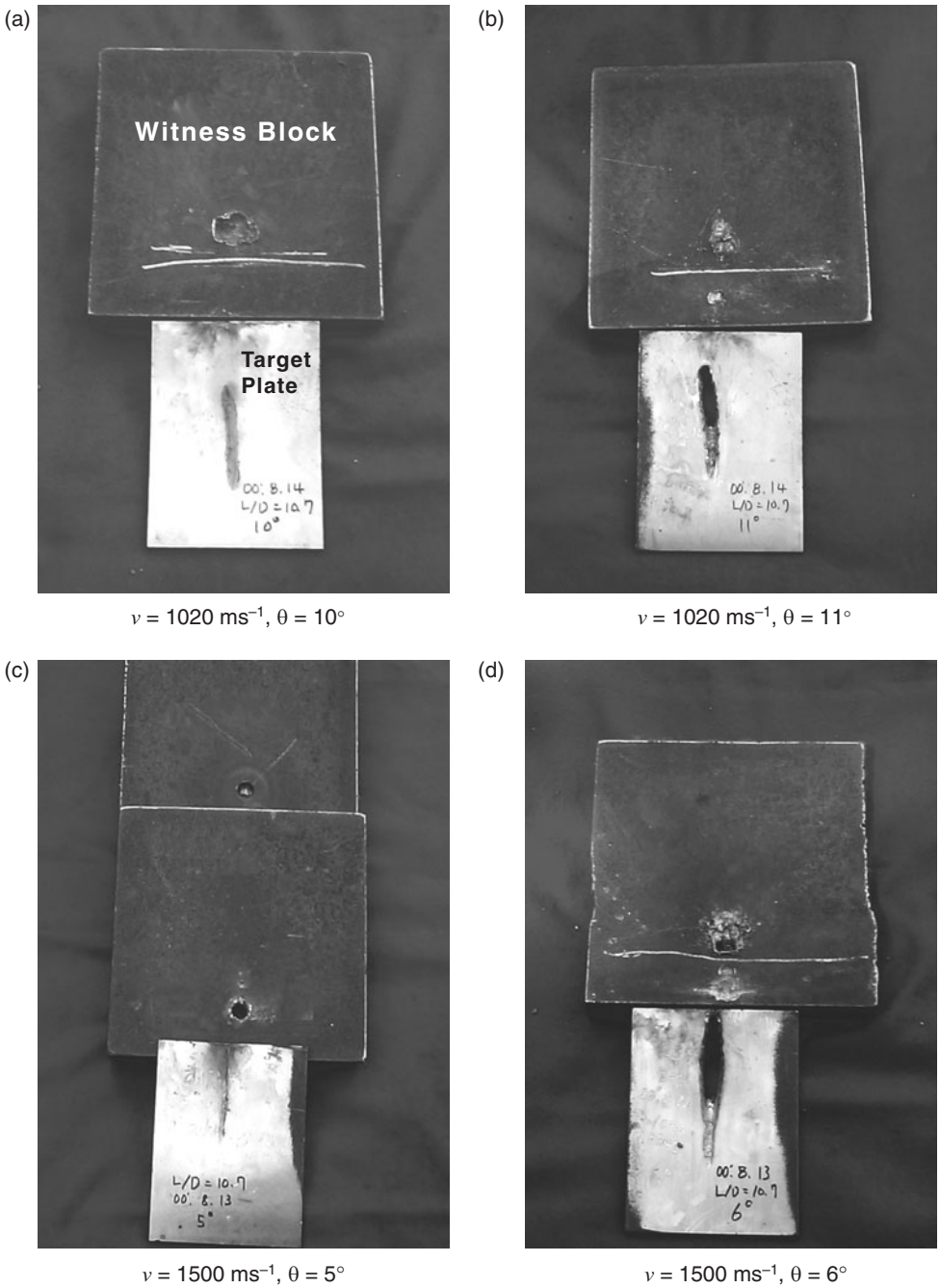

Figure 8. Photographs showing the results from ricochet experiments.

observing deformed and eroded surfaces of the target plate and penetration holes in the witness block. When a projectile impacted the target plate having oblique angles lower than some critical value, as can be seen in figures 8(*a*) and (*c*), the ricochet process resulted in a long surface groove in the target plate formed by erosion, and in a single penetration crater on the witness block. At an oblique angle slightly higher than the critical value, however, the projectile broke into two parts, resulting in a characteristic phenomenology in the target plate and the witness block shown in figures 8(*b*) and (*d*): there is an apparent groove (crater) followed by a single perforation hole in the target resulting from initial erosion and a subsequent penetration whilst two penetration holes are noticeable in the witness block, one over and the other below the white line in figures 8(*b*) and (*d*) where the edge of the target was located.

The post-impact behaviour of the deformable projectile and the deformable target with finite thickness described so far in general agrees qualitatively with what has been observed and predicted in the previous works in which ricochet occurred at undeformable (and sometimes rigid) target surfaces [6–12]. However, as apparent in figures 4–6, the inward deformation of the target plate due to the finite thickness comparable to the projectile diameter is shown to assist the segmentation of the projectile, followed by the perforation of the target plate by the broken rear part of the projectile. Such phenomena

could be responsible for the difficulty of obtaining ricochet from relatively thin plates.

4.2. Critical ricochet angles

In accordance with the definition of ricochet mentioned in the introduction, changes in the critical ricochet angles were derived by analysing the numerical results graphically in the manner described in section 4.1 and were plotted as functions of impact velocities in figure 9 for the RHA target plate. The ricochet angle curves shown in figure 9 were obtained from curve-fitting the numerical results as a first-order exponential decay function. The fitted equations, their parameter values, and the statistical analysis of the fitted results are also reported in the figure. The numerical results are confirmed with experimental results as shown in figure 9. In figure 9, the hollow square markers indicate perforation of the RHA target plate by the long-rod projectile whilst the solid square markers indicate critical ricochet of the projectile. It can be seen that there is good agreement between the two.

It is noticed in figure 9 that the critical ricochet angle falls with increasing impact velocities. In other words, at a low target oblique angle, the ricochet can be achieved up to relatively high impact velocities though the penetration capability in flight direction is high at such velocities, i.e. ricochet is easily achieved with a low oblique angle. On the other hand, when the target oblique angle is high, the ricochet is possible only up to a limited impact velocity beyond which full penetration (perforation) occurs.

Such a trend—increasing ricochet angles with lower impact velocities—can be understood from the pressure (or axial stress) developed at the projectile–target interface, known as Tate pressure, which takes the form of a modified Bernoulli equation as [14, 15, 41]:

$$\hat{P} = \tfrac{1}{2}\rho_{\mathrm{p}}(v-u)^2 + Y_{\mathrm{p}} = \tfrac{1}{2}\rho_{\mathrm{t}}u^2 + R_{\mathrm{t}} \qquad (5)$$

As a rough approximation, if it is assumed that no penetration of the target occurs unless the impact velocity v exceeds a certain critical value, the penetration velocity u will be zero when a projectile impacts at critical velocity. Hence, by substituting u with 0, the critical velocity, v_{cn}, for normal impact is now obtained from equation (5) as [6]

$$v_{\mathrm{cn}} = \sqrt{\frac{2(R_{\mathrm{t}} - Y_{\mathrm{p}})}{\rho_{\mathrm{p}}}} \qquad (6)$$

where v_{cn} is the constant which consists of the material constants for the two materials. When the target is inclined with oblique angle θ as shown in figure 1, by analogy, it can be assumed that ricochet would occur if the normal component of the projectile velocity, $v\sin\theta$, does not exceed a certain constant value, K, similar to the right-hand side in equation (6). Then, critical impact velocity for ricochet, $v_{\mathrm{co}}\sin\theta$, for oblique impact can be expressed as

$$v_{\mathrm{co}}\sin\theta = K \qquad (7)$$

Such a simple conceptual relation qualitatively explains why a higher oblique angle is allowed for ricochet at a lower impact velocity. However, since the ricochet is a much more complicated, three-dimensional phenomenon, the actual dependence of ricochet angle on the impact velocity shown in figure 9 is somewhat more pronounced than in this simple qualitative model.

The numerical results on the critical ricochet angles are also compared with existing two-dimensional analytical models developed by Tate [6] and Rosenberg *et al* [7], independently. The critical ricochet angles based on these models have been calculated for a WHA long-rod projectile and a RHA target as functions of impact velocities in figure 10. Also shown are the corresponding numerical results. It can be seen in the figure that the Tate model overestimates the critical ricochet angle for impact velocities higher than $1070\,\mathrm{m\,s^{-1}}$ and *vice versa* for lower velocities. Further, the slope of the Tate curve is different from the numerical one: the difference in the two curves becomes larger as the velocity of interest either increases or decreases from $1070\,\mathrm{m\,s^{-1}}$. On the other hand, the model developed by Rosenberg *et al* shows a similar trend to the numerical results, though the former overestimates the critical ricochet angles at all impact velocities. However, if it is shifted vertically downward in figure 10, Rosenberg *et al*'s model coincides closely with

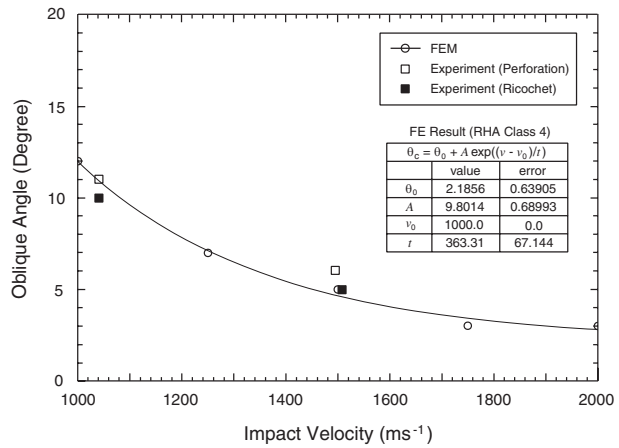

Figure 9. Comparison of the numerically predicted critical ricochet angles for various velocities with the experimental results.

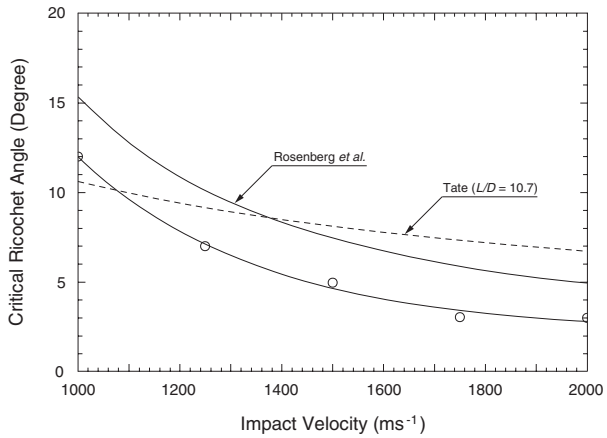

Figure 10. Comparison of the numerically determined critical ricochet angles for various velocities with those predicted from two-dimensional analytic models of Tate [6] and Rosenberg *et al* [7].

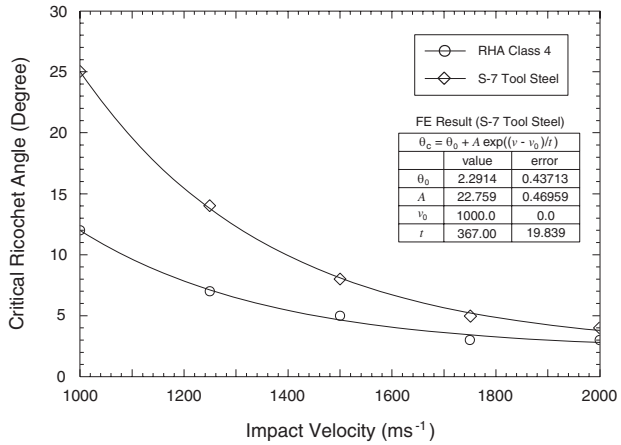

Figure 11. Effect of target strength on the critical ricochet angles.

the numerical results and therefore their analytical model can be used as a practically useful guideline to estimate ricochet angles if used with care.

4.3. Effects of the target strength

Whilst the RHA has been widely used as a primary armour material over decades, in some cases, stronger material such as high hardness armour (HHA) has also been adopted, though its use is limited due to lower toughness. To investigate the effect of material strength on the ricochet angle, material constant terms in the Johnson–Cook model for S-7 tool steel, which has static yield strength and hardness similar to HHA produced by ThyssenKrupp AG, were taken from the literature [36] and applied to the numerical model. The ricochet angles calculated for S-7 tool steel were plotted as a function of the impact velocity in figure 11. Numerical results have been curve-fitted using first-order exponential decay function as in the case of RHA. It can be seen that a higher ricochet angle is predicted for a given impact velocity if the target strength is increased. Such behaviour is explained by examining the one-dimensional hydrodynamic penetration model described in equation (5). Resistance of an oblique target material to penetration in the vertical direction, i.e. the constant K in equation (7), consists of contributions from the inertia term (function of penetration velocity and density of target medium) and the material strength term[3]. Taking the inertia terms for RHA and S-7 tool steel to be the same due to the similar densities of these materials, it is expected that the only difference in the penetration resistance in the vertical direction will result from the material strength term. It was reported that the dynamic yield strengths, R_t, of S-7 tool steel and RHA are about 6.2 and 5.3 GPa, respectively [42]. Thus, at a given impact velocity, use of the high hardness plate, S-7 tool steel, would foster the ricochet of the projectile, i.e. the target plate can tolerate more vertical component of the projectile movement. This implies that the target plate with higher strength allows a higher oblique angle for the ricochet of the projectile at a given velocity.

It is further noticed in figure 11 that there is a salient increase in the ricochet angle especially at low impact velocities as the material strength increases whilst improvement in ricochet capability through the use of stronger materials gradually decreases at higher velocities. Such a trend is qualitatively predicted when the constant in equation (7), which is related to the dynamic strength of the target material, is changed to a higher one for the S-7 tool steel.

[3] In the case of a fluid target, the inertia term is the only resistance mechanism of the target against the vertical component of the projectile movement.

5. Summary and conclusions

Ricochet of a WHA long-rod projectile impacting on oblique, steel target plates with finite thickness was investigated numerically using a full, three-dimensional, explicit finite element method with supplementary experiments. Effects of the impact velocities of the projectiles and the hardness of the plates on the critical ricochet angle were considered.

It was predicted in the numerical analysis that the projectile and the target behave in three different ways depending on the oblique angle of the target. For a relatively low oblique angle, the impacted projectile bent and slid on the target surface to bounce away with very little velocity drop whilst no significant deformation of the target was predicted. With increasing oblique angle, the projectile initially bent on impact but the target deformed substantially to arrest the tail portion of the target behind the plastic hinge. This resulted in the projectile stretching between the head and the tail, which pulled the tail out of the target to achieve critical ricochet. Segmentation of the projectile then followed. When the oblique angle was further increased, the projectile impact caused severe target cratering which played the role of guiding the tail portion of the projectile through the target resulting in perforation. In this case the projectile broke before its head left the target. Such behaviour of the projectiles and the target plates predicted in this numerical study was supported by experimental observations of the deformed shape of the target plates and the penetration holes on the witness blocks. The post-impact behaviour of the deformable projectile and deformable target with finite thickness in this work in general agreed qualitatively with previous work based on undeformable (and rigid) target surfaces. However, the deformable target assisted the breakage of the projectile followed by the perforation of the plate by the broken rear part of the projectile.

Critical ricochet angles were also derived from the numerical analysis. For the cases considered herein, the numerical study predicted that the critical oblique angle of the target plates required for ricochet of long-rod type projectiles rises with lower projectile velocity and the prediction was shown to be reliable by experimental results. This trend itself is consistent with a two-dimensional analytical model whilst it was suggested that the two-dimensional results are an overestimation, which is qualitatively consistent with the results of Zukas and Gaskill [9]. When the target hardness was considered, the numerical results predicted that a higher ricochet angle can be obtained by employing harder target materials for a given impact velocity, which was appreciable at lower velocities in particular.

References

[1] Zukas J A 1990 *High Velocity Impact Dynamics* (New York: Wiley)

[2] Ogorkiewicz R M 1991 *Technology of Tanks* (Coulsdon: Janes's Information Group)
[3] Goldsmith W and Cunningham D M 1956 *J. Appl. Mech. (Trans. ASME)* **78** 612
[4] Recht R F and Ipson T W 1962 The dynamics of terminal ballistics *Final Report* No AD274128 (Denver: Denver Research Institute)
[5] Finnegan S A, Dimaranan L F, Heimdahl D E R and Pringle J K 1993 *Proc. 14th Int. Symp. Ballistics* p 661
[6] Tate A A 1979 *J. Phys. D: Appl. Phys.* **12** 1825
[7] Rosenberg Z, Yeshurun Y and Mayseless M 1989 *Proc. 11th Int. Symp. Ballistics* p 501
[8] Senf H, Rothenhausler H, Scharpf F, Both A and Pfrang W 1981 *Proc. 6th Int. Symp. Ballistics* p 510
[9] Zukas J A and Gaskill B 1996 *Int. J. Impact Eng.* **18** 601
[10] Johnson W, Sengupta A K and Ghosh 1981 *Int. J. Mech. Sci.* **24** 425
[11] Johnson W, Sengupta A K and Ghosh 1981 *Int. J. Mech. Sci.* **24** 437
[12] Reid S R, Edmonds A J and Johnson W 1981 *J. Mech. Eng. Sci.* **23** 85
[13] Jonas G H and Zukas J A 1978 *Int. J. Eng. Sci.* **16** 879
[14] Tate A 1967 *J. Mech. Phys. Solids* **15** 387
[15] Tate A 1969 *J. Mech. Phys. Solids* **19** 121
[16] Tate A 1977 *Int. J. Mech. Sci.* **28** 535
[17] Goldsmith W and Finnegan S A 1986 *Int. J. Impact Eng.* **4** 83
[18] Roecker E and Grabarek C 1986 *Proc. 9th Int. Symp. Ballistics* p 467
[19] Falcovitz J, Mayseless M, Tauber Z, Keck D, Keneddy R, Ofstedahl K and Sing P 1989 *Proc. 11th Int. Symp. Ballistics* p 311
[20] Johnson G R, Stryk R A, Holmquist T J and Souka O A 1990 *Int. J. Impact Eng.* **10** 281
[21] Cullis I G and Lynch N J 1995 *Int. J. Impact Eng.* **17** 263
[22] Luttwak G, Rosenberg Z and Kivity Y 1996 *AIP Conf. Proc.* p 370
[23] Pierazzo E and Melosh H J 2000 *Ann. Rev. Earth Planet. Sci.* **28** 141
[24] Hohler V and Stilp A J 1981 *Proc. 6th Int. Symp. Ballistics* p 333
[25] Sislby G F 1984 *Proc. 8th Int. Symp. Ballistics* p 31
[26] Cagliostro D J, Mandell D A, Schwalbe L A, Adams T F and Chapyak E J 1990 *Int. J. Impact Eng.* **10** 81
[27] Bjerke T W, Silsby G F, Scheffler D R and Mudd R M 1992 *Int. J. Impact Eng.* **12** 281
[28] Bukharev Y I and Zhukov V I 1995 *Comb. Expl. Shock Waves (Fiz. Goren. Vzryva)* **31** 362
[29] Goldsmith W, Tam E and Tomer D 1995 *Int. J. Impact Eng.* **16** 479
[30] Anderson C E, Bless S J, Sharron T R, Satapathy S and Normandia M J 1998 *AIP Conf. Proc.* p 925
[31] Lee M and Bless S J 1998 *AIP Conf. Proc.* p 929
[32] Zienkiewicz O C and Taylor R L 1991 *The Finite Element Method* 4th edn, vol 2 *Solid and Fluid Mechanics/Dynamics and Non-linearity* (New York: McGraw-Hill)
[33] Belytschko T, Liu W K and Morgan B 2000 *Nonlinear Finite Elements for Continua and Structures* (New York: Wiley)
[34] Goldsmith W 1999 *Int. J. Impact Eng.* **22** 95
[35] US DoD 2000 *Armour Plate, Steel, Wrought, Homogeneous* Military Specification MIL-A-12560H (Amendment 3)
[36] Johnson G R and Cook W H 1983 *Proc. 7th Int. Symp. Ballistics* p 541
[37] Meyers M A 1994 *Dynamic Behavior of Materials* (New York: Wiley)
[38] DYTRAN User's Manual 2001 (Los Angeles: MacNeal-Schwendler Corp.)
[39] Rosenberg Z and Dekel E 1998 *Int. J. Impact Eng.* **21** 283
[40] Anderson C E, Walker J D, Bless S J and Partom Y 1996 *Int. J. Impact Eng.* **18** 247
[41] Anderson C E and Walker J D 1991 *Int. J. Impact Eng.* **11** 481
[42] Anderson C E, Walker J D and Hauver G E 1992 *Nucl. Eng. Design* **138** 93